Propulsion and Energy Forum
July 25-27, 2016, Salt Lake City, UT
52nd AIAA/SAE/ASEE Joint Propulsion Conference

Mass Spectrometry of Selected Ionic Liquids in Capillary Electrospray at Nanoliter Volumetric Flow Rates

Shawn W. Miller[1]
Boston College, Institute for Scientific Research, Chestnut Hill, MA, 02467

Benjamin D. Prince[2] and Raymond J. Bemish[3]
Air Force Research Laboratory, Space Vehicle Directorate, Kirtland AFB, NM, 87117

and

Joshua L. Rovey[4]
Missouri University of Science and Technology, Rolla, MO, 65401

Capillary-based electrospray thrusters allow user-enabled control of the volumetric flow rate of the propellant. This control, coupled with mass spectrometry techniques spanning a large mass-to-charge range, enables elucidation of the composition of the electrospray beam and through further analyses, a better understanding of the physics occurring at the liquid/vacuum interface. In this work, mass spectra of selected ionic liquids electrosprayed from a capillary emitter are measured, using time-of-flight mass spectrometry, over a wide range of volumetric flow rates. The time-of-flight mass spectrometer enables simultaneous acquisition over a mass-to-charge range of 20 amu/q to ~500,000 amu/q in a single pulse cycle. Additionally, the use of orthogonal extraction enables direct determination of the kinetic energies of ions present in the electrosprayed beam. The presented data reveal a complex emission process occurring for ionic liquid capillary-based electrospray at nanoliter volumetric flow rates. The electrospray beam mass-to-charge composition includes a sequence of singly-charged ions and doubly-charged ions at nearly all sampled flow rates for all electrosprayed ionic liquids. In addition to the small ion-clusters, two Maxwell-Boltzmann distributions from approximately 10,000 amu/q to 500,000 amu/q exist in the spectra each with mass-to-charge distribution sensitive to the volumetric flow rate. The volumetric flow rate dependence of the largest charge-to-mass ratio droplets appears to be consistent with previously measured scaling laws, although exhibiting a wide mass-to-charge distribution. The flow rate dependence of the lower mass-to-charge distribution is more complex and is discussed in some detail. Measurement of the time-of-flight mass spectrum for a number of different ion kinetic energy defects over a number of different volumetric flow rates results in a more thorough understanding of kinetic energy losses experienced in the jet structure of the Taylor cone, with direct impacts to the thrust performance of these types of devices. The appearance of these ions and distributions alter the thought on the emission mechanism at work in the electrospray system. No longer is electrospray defined and easily explained by the Iribarne emission mechanism and droplet generation by the Rayleigh instability.

[1]Research Associate, Institute for Scientific Research, St Clement'sHall 402, 140 Commonwealth Ave, and Member AIAA.
[2]Research Chemist, Space Vehicles Directorate, 3550 Aberdeen Building 570, and Member AIAA.
[3]Senior Research Chemist, Space Vehicles Directorate, 3550 Aberdeen Building 570.
[4]Associate Professor of Aerospace Engineering, Mechanical and Aerospace Engineering, 292D Toomey Hall, 400 W.13th St, Associate Fellow AIAA.

Nomenclature

m	=	mass
q_{Ray}	=	charge at Rayleigh limit
r_{Drop}	=	droplet radius
γ	=	surface tension
ε_0	=	permittivity of free space
ρ	=	density

I. Introduction

ELECTROSPRAY thrusters constitute a class of micro-electric propulsion systems that use an electric field to evaporate and accelerate an ionic propellant to generate thrust. This class of thruster is ideal in operations that require precise, low thrust levels while still efficiently utilizing the stored propellant (e.g. high specific impulse (I_{SP})). Electrospray thrusters do not rely on capacitor charging, are free of electrical discharges, and allow use of both polarities of ions in its operation. An additional advantage is that some ionic liquid propellants can be used in a dual-mode or dual-use propulsion system where common hardware and propellant are used to combine different propulsion systems together. In a dual-mode system, the electrospray thruster is expected to fulfill the mission requirement for lower thrust, high I_{SP} precision maneuvering.

Current state-of-the-art electrospray systems typically employ ionic liquids as their propellants of choice. Ionic liquids (ILs) are molten salts with melting points below 100 °C. As a liquid, ILs are quasi-neutral with both cations and anions dispersed throughout the fluid and these charged species are extracted under strong electric field conditions. ILs have advantageous physical properties including high conductivity (>1.0 S/m), low viscosity (<50 cP), and very low vapor pressure (No vaporization in vacuum). Some ILs are even more ideal because of the combustive properties of the liquids, which have the potential to be hydrazine replacements for chemical systems. The proposed work that follows includes one IL that is known to be hypergolic with white fuming nitric acid.[1] These types of ionic liquids serve as the propellant in current state-of-the-art IL electrospray thrusters, which employ either a surface wetting (needles) or internally wetting (capillaries) flow path emitter. Busek Co. Inc. designed, tested, and operated an ionic liquid capillary system for the NASA LISA (Laser Interferometer Space Antenna) mission before its ultimate cancelation.[2-4] State-of-the-art needle-style emitters include the scalable ion Electrospray Propulsion System (s-iEPS), which was recently delivered to NASA for use as a propulsion system for cubesats.[5]

Mass spectra of ionic liquid electrospray thruster systems have been reported in the literature for both styles of emitters operating in the low mass-to-charge regime. For needle-style emitters using ionic liquid propellants, typical reports of mass spectra include either pure ions or perhaps an ion with a single neutral pair.[6] Additionally, there are reports of the same ions with small mass-to-charge droplets in the 10,000's of amu/q range, where the droplet's mass-to-charge has been determined from near-field quartz-crystal microbalance (QCM) and faraday cup (FC) measurements.[7] Alteration of the needle emitter surface has been shown to impact the intensity ratio of ion species as well as the quantity and mass-to-charge of droplets emitted, again determined through the use of near-field measurements.[8, 9] This alteration is likely the result of flow rate modification of the ionic liquid propellant, although no direct measurement of the flow rate was possible. We have previously reported on the effects of volumetric flow rate on the emitted ion species from a capillary-style emitter employing the ionic liquid BMI-DCA (1-butyl-3-methylimidazolium dicyanamide).[10, 11] At the lowest flow rates sampled, the smallest ion species appeared to be the most intense as measured through quadrupole mass spectrometry with an upper m/q range of 1,000 amu/q. As the flow rate was increased, the presence of larger ion clusters such as the n = 3, 4, and 5 cations (i.e. 3, 4 and 5 neutral pairs attached to a single BMI cation) became more apparent. Near-field measurements suggested that large mass-to-charge (m/q) species existed with m/q values ranging from approximately 95,000 amu/q at 0.3 nL/s to ~250,000 amu/q at 2.18 nL/s. Recently, Terhune *et al.* have reported on the volumetric flow rate impacts of adding magnetic fields to ionic liquids infused with ferrofluid nanoparticles operated in capillary electrospray systems using the same orthogonal time-of-flight mass spectrometry system as this work.[12] The fact that the volumetric flow rate influences the emitted ions is, by this point, well known in the literature despite the reliance on QCM and FC type devices to report the average value of the m/q ratio. In this work, we aim to directly measure, as opposed to inferring from near-field measurements, the volumetric flow rate dependence of the emitted ions through time-of-flight mass spectrometry.

Previous investigations of needle and capillary electrospray emitters at the Air Force Research Laboratory using quadrupole mass spectrometry coupled with retarding potential analysis (RPA) have noted that the presence of large mass-to-charge droplets near the center emission axis have also been correlated with reduced kinetic energies of the ions, as compared to the bias potentials applied to the emitters.[10, 11, 13] These losses are typically termed "ohmic losses" and are understood to occur as a result of jet extension from the Taylor cone structure. These losses impact the

thrust performance of the device through a reduction in the net acceleration of the ion, as compared to the theoretical maximum. The combined quadrupole/RPA experiments referenced above were only capable of providing ion-specific RPA analyses for those ions below 1,000 amu/q; any larger *m/q* value was simply aggregated into one profile, assuming it successfully passed through the quadrupole operating in all-pass operation. These distributions tend to cover a broad energy range and can cover 100's of electronvolts (eV) for a 500 V bias potential. The breadth of the energy distributions might be reflective of a diverse number of emission positions on the jet, such as emission from the side of the jet versus the tip, or be a consequence of the dynamics occurring in the jet itself. Kinetic energy selective orthogonal time-of-flight mass spectrometry will be used to examine the resulting mass spectrum of ions in narrow kinetic energy bands.

Ionic liquids constitute a very wide chemical phase space, with a number of liquids that might make suitable electrospray propellants. The situation becomes even more complex when ionic liquid mixtures are included, such as those liquid mixtures considered for dual-mode application.[14] This work will consider a variety of ILs with different cations and anions. The intention is not to determine the best propellant for electrospray thrusters but instead provide a firmer foundation from which to model the emission behavior. A sampling of unique cations and anions enables an assessment of the generalities from the observations and ensure that the observations are not unique to a particular chemical.

In this work, we present quadrupole and orthogonal time-of-flight mass spectrometry results over a wide range of volumetric flow rates for a number of ILs with different cations and anions emitted from a capillary electrospray emitter. The orthogonal time-of-flight investigations also examine the mass spectrum of the emitted ions at a specific kinetic energy yielding insights into the energy dependence of the various emitted ions at a given volumetric flow rate. In Section II, we describe the experimental details and identify the selected ionic liquids studied. The mass spectrometric results for the various ionic liquids are given in Section III. Finally, the results are discussed in Section IV.

II. Experimental

The electrospray source in both setups was identical and has been described in previous works.[10, 11] The source was simply the pairing of an extractor plate with a 1.5 mm diameter aperture and a conductive emitter (i.e. metal-coated fused-silica capillary at 50 μm diameter) set approximately 1.5 mm apart. The ion source operated with either a ±500 or ±900 V emitter potential per each experimental setup. The quadrupole instrumentation used the ±500 emitter potential while the time-of-flight experiment used the ±900 V emitter potential. The potential applied to the extractor varied by the IL used but was chosen so as to be close to the turn-on voltage required for the specific IL. The IL volumetric flow rates were determined by using the rate at which a bubble traveled over a fixed length in the IL supply capillary. The results were fit to a linear relationship linking reservoir pressure to volumetric flow rate. Variable flow rates were selected by varying the IL reservoir backing pressure. The IL reservoir backing pressure and associated incremental pressure steps were identical for all ILs. The volumetric flow rate of an IL depends on the ILs physical properties and may be larger or smaller relative to another IL for a given pressure. For example, BMI-IM was examined for rates from 0.46 to 1.46 nL/s while EMI-IM was examined for rates from 0.09 to 2.35 nL/s. In the results section, a few sample flow rates are presented for each IL to illustrate the behavior of the IL electrospray beam.

The focus of the capillary electrospray was on ILs featuring the EMI and BMI cations (1-ethyl-3-methylimidazolium and 1-butyl-3-methylimidazolium) paired with the anions of BF_4, IM, and DCA (tetrafluroborate, bis(trifluromethylsulfonyl)imide, and dicyanamide). These commonly electrosprayed ILs were selected for known ease at being electrosprayed and for already published worked on mass comparison at lower mass ranges (i.e. < 1,200 amu/q). The masses of these are as follows: EMI^+ at 111 amu, BMI^+ at 139 amu, BF_4^-at 87 amu, IM^- at 280 amu, and DCA^- at 66 amu.

This study of IL electrospray used two different experimental systems. The first system was a quadrupole mass spectrometer capable of measuring the intensity of the charged species in the electrosprayed beam out to 3,750 amu/q. This system was similar to that featured in the work by Chiu *et al.*, but with an improved mass scanning range extended from 1,000 amu/q to 3,750 amu/q.[7, 13, 15, 16] Current, mass flux, and retarding potential data could be collected from this instrument, but was not extensively utilized for this paper. The quadrupole was used to aide in resolving the smallest and least charged species emitted. Visual inspections of the steadiness of the Taylor cone at the operating voltage and flow rate were conducted and the operating conditions recorded for continuity with the other mass spectrometer system. The quadrupole instrument featured in Fig. 1 illustrates the rotating electrospray source and linear flight path through the quadrupole setup. The ion detector consisted of an off-axis channeltron paired to a pre-amplifier and discriminator. The intensity of a specific *m/q* species was counted by means of an event counter. A large

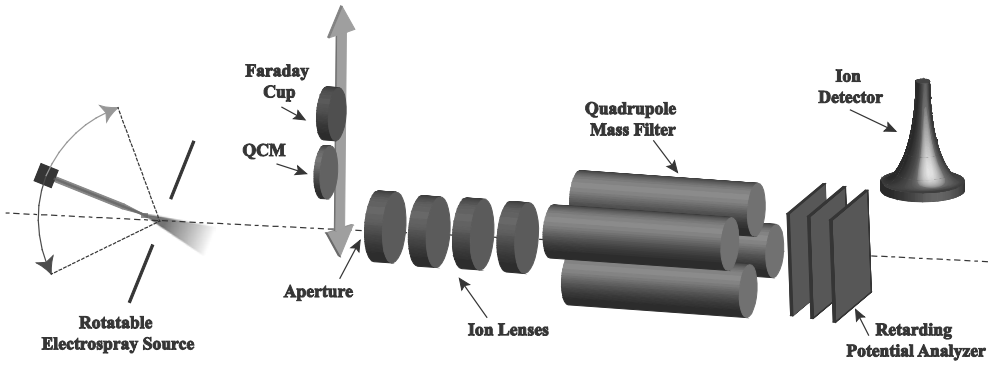

Figure 2. Schematic diagram of the quadrupole mass spectrometer instrument.

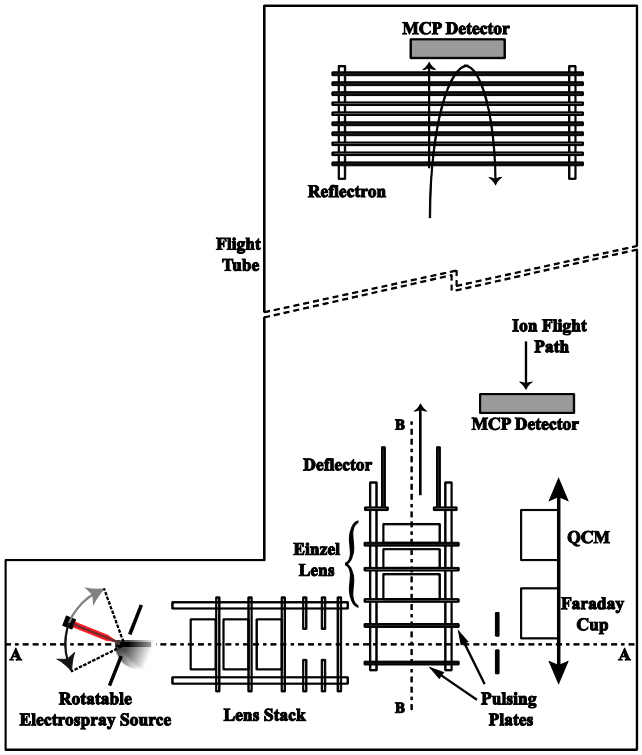

Figure 1. Orthogonal TOF experimental setup featuring translating Faraday cup and QCM. The ion beam flight occurs along axis A-A, but the pulsing plates redirect the ion beam along axis B-B into the TOF flight tube.

"zero-mass" peak extending to ~100 amu/q is the result of the high kinetic energy of the emitted ions and the large mass range of the quadrupole mass spectrometer.

An orthogonal time-of-flight (TOF) instrument was the second and primary system used for this study. Figure 2 illustrates the setup of this experimental system. Emitted ions are extracted from the source region and introduced into a lens stack composed of lenses and deflectors whose potentials are adjusted to maximize throughput through a slot centered at the far end of the pulsing plates. The current and mass flux passing through the slot are measured via a translating Faraday cup and quartz crystal microbalance (QCM). The two pulsing plates are separated by approximately 13 mm and make up the extraction region for the mass spectrometer. The two plates, termed the repeller (bottom) and extractor (top), are independently given potentials. The extractor plate has a circular aperture of radius 6.5 mm covered with a mesh grid. The two plates first serve as low energy bandpass filters by applying the same potential to both plates. For example, for a +900 V emitter bias, applying a +700 V potential to both plates will allow only those ions with at least 700 eV/q to pass through the extraction region in the axial direction. As a result, only those ions with a kinetic energy defect of less than 200 eV/q are permitted to pass in the axial direction, under the example circumstances.

Orthogonal (i.e. transverse) extraction of the axially-moving ions occurs through the application of an additional potential to the repeller plate. This additional potential is typically +375 V (i.e. +1075 V net, in the example above) and is applied to the repeller plate for either 10 µs or 100 µs at a repetition rate of 250 Hz in these experiments. Orthogonally extracted ions are then accelerated in a second stage between the extractor plate and the front plate of an Einzel lens downstream 70 mm, where the front plate is held at ground potential. The second lens of the Einzel stack serves to focus the extracted beam downstream and the orthogonally extracted ion beam passes through the final grounded element of the Einzel stack. Beyond the Einzel stack, the ion beam passes through a deflector after which the beam enters the field-free region of the time-of-flight mass spectrometer. At the end of the ~1.0 meter flight tube, a series of grids serves to reflect the ion beam. The reflected ion beam impinges on a multi-channel plate (MCP) and is counted by means of a pre-amplifier attached to a time-of-flight counter card. The Einzel lens, deflector, and reflectron potentials were determined by maximizing the amplitude and minimizing the linewidth of the smallest ion species for each pulsing plate potential value.

The time-of-flight mass spectra shown in the results section of this paper include ions with *m/q* values exceeding 200,000 amu/q. It must be noted that such species transverse velocities increase significantly slower than those of much smaller *m/q* values. For a 10 μs pulse and an ion beam centered between the two pulsing plates with a full-width half maximum distribution of 1.25 mm, simulations indicate that *m/q* values above 20,000 amu/q will begin to be attenuated (i.e. the pulse will end before the species escapes through the extractor plate). This attenuation results in just 5% of ions with 400,000 amu/q reaching the theoretical maximum of transverse velocity. The pulsing system supplied with the Jordan reflectron TOF mass spectrometer was only capable of delivering pulses of 1-10 μs in duration. During the acquisition of the data for this report, a longer duration pulser unit was acquired. As a result, data from both pulsing units are described. A comparison of the two pulsers will be presented in the results section. One final consideration regarding the measurements made in this report pertains to the notion of energy-selected time-of-flight mass spectrometry.

We have performed extensive simulation of ion flight in the orthogonal time-of-flight instrument using the exact geometries of the instrument. Among the most important findings of these simulations pertains to the axial kinetic energies of those ions that can be orthogonally extracted. In the extraction region, the pulsing plates are provided a base potential. This potential serves to retard the axial velocity of the ion beam as the ions enter the extraction region. If an ion retains a significant axial velocity upon pulsing, it is likely to collide with either the extractor pulsing plate or the various walls and fail to reach the detector. We find that ions, irrespective of ion mass, with axial velocities greater than 20 eV/q after subtraction of the base pulsing plate potential cannot successfully reach the detector.

III. Results

This section is divided into three parts based on the anion component of the ILs studied. Each section will provide a briefing on the data presented with further analysis following in the discussion. This study picks up from the previous work of the Air Force Research Laboratory in reference [11] where unknown charged masses above 1,000 amu/q emitted from a BMI-DCA electrospray beam were influencing the performance output of the electrospray. The retarding potential analysis of BMI-DCA indicated that these higher massed species originated at a potential approximately 50% of the capillary bias potential. This RPA information suggested that the TOF instrument should be operated at 50% of the bias potential to fully capture these higher massed species. The orthogonal TOF instrument selects and separates charged species of a beam by a defined potential instead of allowing ions at all potentials down the flight path. The pulsing plates set at this constant potential retards the electrospray beam slowing the ions at or near this potential to zero velocity. The application of an additional pulse voltage (nominally 375 V) redirect these slowed ions into the TOF flight tube with a new uniform potential equal to the total pulse voltage. In setting the TOF operation at the 50% potential, the discovery was made that 50% of the capillary bias potential also occurred at the 50% of the electrospray beam current. 50% of the beam current was a readily available and observable value unlike the RPA value, which required additional testing to verify for each IL and flow rate. TOF data in the following sections were collected on all ILs using this operation scheme unless otherwise stated.

A. IM-Based ILs

Figures 3 and 4 show the mass spectra of the two IM-based ILs acquired with both the orthogonal time-of-flight instrument and the quadrupole mass spectrometer. Figure 3a presents the cation TOF for the BMI-IM system acquired at an energy defect of 350 eV/q, or an equivalent pulsing plate potential of 550 V for a 900 V emitter potential. As an example, an energy defect of 50 V means the base potential of the pulsing plates has been set at 50 V below the emitter bias with the result of only allowing ions with axial kinetic energies greater than 850 eV/q, in this experiment, to pass through the extraction region, The TOF instrument only allows ions within 20 eV/q of the defect to be introduced into the flight tube. The BMI-IM TOF results are depicted for flow rates ranging from 0.46 nL/s to 1.46 nL/s. At the lowest flow rate of 0.46 nL/s, there is only evidence of small mass ion species and a single Maxwell-Boltzmann distribution centered near 40,000 amu/q. As the flow rate is increased, this low *m/q* distribution, assumed to represent a lower mass droplet, narrows and shifts towards zero and by 0.96 nL/s, a second Maxwell-Boltzmann distribution is clearly evident in the mass spectrum. This second, higher *m/q* distribution is assumed to represent a higher massed droplet. The most probable *m/q* value continues to increase for the large mass droplet as the flow rate increases. The TOF cation mass spectra for the EMI-IM system are shown in Fig. 3b for flow rates ranging from 0.09 to 2.35 nL/s. At a flow rate of 0.09 nL/s, only $n = 0$ through, perhaps, $n = 7$ (i.e. 2848 amu/q) are detectable. At higher flow rates, the two Maxwell-Boltzmann distributions develop and persist in the spectra.

Similarly to the BMI-IM system, the low mass droplet distribution, when present, starts out centered at larger *m/q* value and exhibits a wider full width half maximum (FWHM) but as the flow rate increases, the most probable value of the distribution shifts to lower *m/q* and the distribution simultaneously narrows and becomes less intense. During this narrowing process, the second distribution peak is observed to increase the most probable *m/q* value with increasing volumetric flow rate. In the inset plots, narrow ion peaks are seen at each of the singly-charged ions out to the $n = 11$ species (4748 amu/q) for BMI-IM and $n = 15$ species (5976 amu/q) for EMI-IM. The intensity of these ions vary with the volumetric flow rate. Beginning at approximately 2,500 amu/q, a new sequence of peaks appears halfway between the singly-charged ions at *m/q* values corresponding to doubly-charged ions. As the volumetric flow rate increases, either the sequence of peaks with *m/q* values above 5,000 amu/q appear to broaden into an unresolvable plateau or two additional peaks have grown to each side of the doubly-charged ions indicating the presence of higher-charged species.

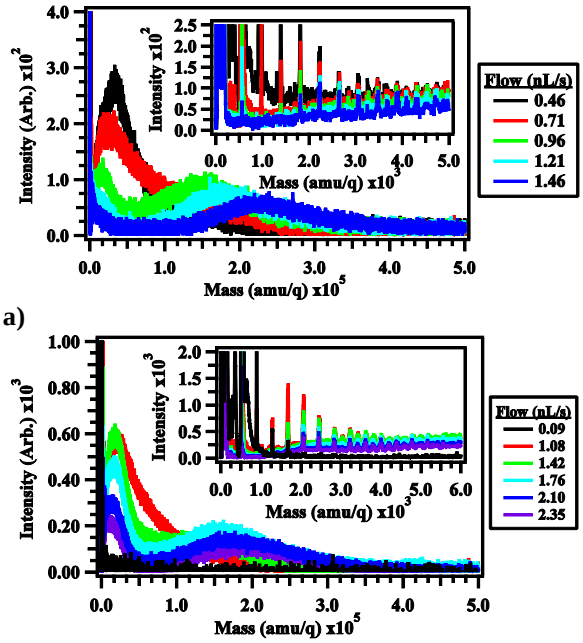

Figure 3. TOF cation mass spectra for the ILs a) BMI-IM and b) EMI-IM. The main plots show the droplet mass range out to 500,000 amu/q, while the inset plots reveals the lower mass ions mass range under 6,000 amu/q.

While no anion mass spectra were collected using the TOF instrument, ions below 3,750 amu/q were available from the quadrupole system. The anion spectra for BMI-IM is shown in Fig. 4a and the EMI-IM system is shown in Fig. 4b. Both exhibit the same pattern in the ions as seen in the TOF cation data, notably, singly-charged ions with doubly-charged peaks appearing in the spectra starting near 2,500 amu/q as the flow rate is increased. In both IM-based systems, the lowest flow rate is dominated by the smallest ion species and increase of the flow rate finds a significant decrease in the $n = 0$ and $n = 1$ intensities which are replaced by large intensities for species near the $n = 4$ ion cluster. While these larger ion clusters are more intense than the smallest ion clusters at higher flow rates, the total intensity of these ions continues to decrease with increasing flow rate.

The energy-selected time-of-flight mass spectra for EMI-IM, with an emphasis on large *m/q* species, are shown in Fig. 5 for energy defects ranging from 50 V to 400 V at a volumetric flow rate of 1.24 nL/s. The ΔV represents the defect value between the emitter bias voltage and the TOF pulsing potential. Figure 5a depicts the mass spectra as-is for a 10 μs pulse. The individual spectra are composed of small ions (not shown), small droplets (~20,000 amu/q), and large droplets that span an approximate range of 100,000 to 400,000 amu/q at this flow rate. The small mass droplets appear to reach peak intensity and peak width near an energy defect of 250 eV/q and are otherwise present at all other sampled energy defects greater than 100 eV/q. The large mass droplets exhibit a significant energy dependency with the largest *m/q* values appearing at the greatest energy defects, although no droplets are observed for the 50 eV/q

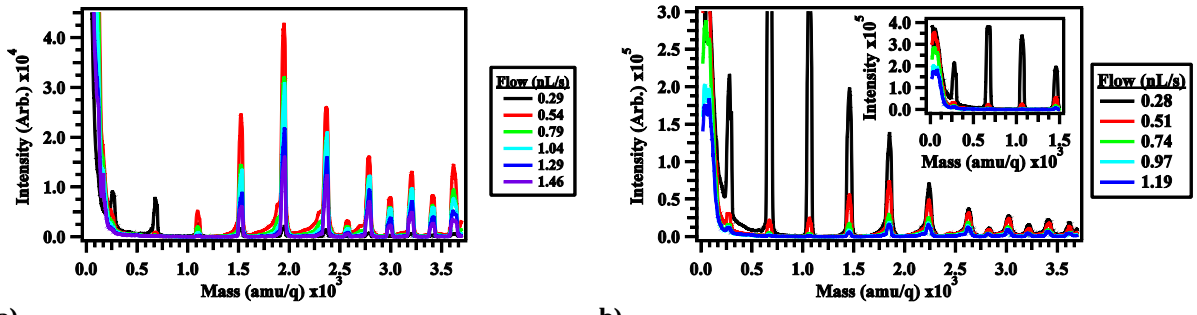

Figure 4. Quadrupole anion mass spectra for the ILs a) BMI-IM and b) EMI-IM. The inset plot illustrates the extended intensity range to show the intensity of the lowest mass ions.

energy defect. As the energy defect is increased, the most probable *m/q* value decreases until an energy defect of approximately 400 eV/q, where the large mass droplets are difficult to distinguish. The largest intensity droplets appear with energy defects near 250 eV/q. Figure 5b illustrates the results of scaling the data shown in Fig. 5a. The data are scaled by dividing a transmission function appropriate for the full velocity extraction from the pulsing region for each *m/q* value for a 10 μs pulse. This transmission function is generated from our modeling and validated later in the Results Section. The main effect of this transmission function is to significantly increase the quantity of large mass droplets detected.

B. BF_4-Based ILs

Of the two BF_4 ILs tested, only BMI-BF_4 was reliably emitted. The electrospray of EMI-BF_4 was not always stable, but the limited quadrupole mass spectra collected revealed two qualitative findings about this IL. The IL is a good source of the unclustered EMI^+ cation, so much so that the detector became saturated by the signal from this one ion when searching for signal from other clustered ions. Additionally, no other singly-charged, fragments, unknown peaks, or doubly-charged/multi-charged ions could be seen in the mass spectra from the quadrupole. Given the difficulty in even achieving limited stable emission, no further tests were performed using the TOF instrument.

Figure 6 shows the quadrupole mass spectra for both the cation and anion cases of BMI-BF_4. The inset plots provide a focused look at the ions under 1,000 amu/q since these ions are more intense than the higher *m/q* ions out to 3,750 amu/q. The flow rate range studied for BMI-BF_4 ranged from 0.12 to 0.67 nL/s over the same reservoir pressure range as the IM liquids, which clearly indicates the influence of a viscous fluid. BMI-BF_4 has a viscosity of 124.0 to 154.0 cP, which is nearly four times that of the IM-based ILs.[17-23] As was with the IM-based ILs, the same pattern in the mass range under 3,750 amu/q is seen in the data. Doubly-charged species appear between the singly-charged ions, but start at lower masses, approximately 1,500 amu/q, with this IL. In both ion polarities, the lowest flow rates have only the first few singly-charged ion peaks, then with increasing flow rate the higher massed, singly-charged ion peaks develop into the mass spectra.

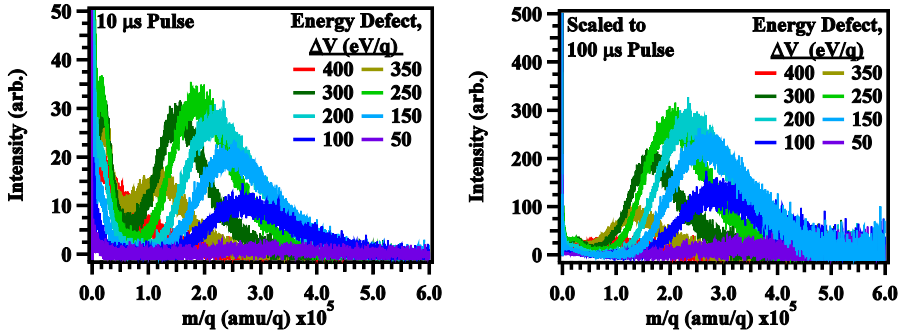

Figure 5. Energy-selective TOF cation mass spectra of EMI-IM droplets at a flow rate of 1.24 nL/s illustrating the a) uncorrected mass spectra with 10 μs pulse and b) scaled mass spectra assuming 100 μs pulse.

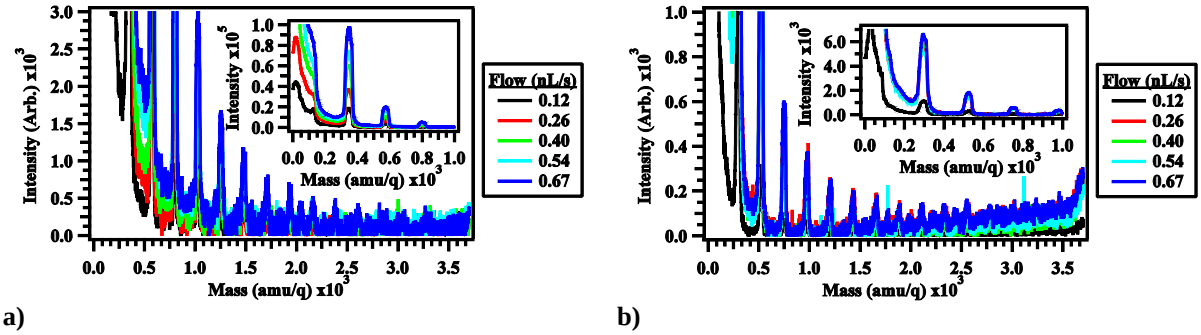

Figure 6. BMI-BF_4 quadrupole mass spectra showing the a) cation spectra and b) anion spectra.

C. DCA-Based ILs

Both EMI-DCA and BMI-DCA were emitted from a capillary emitter, however only BMI-DCA provided useful data and will be presented here. Results from time-of-flight measurements for this liquid are presented in Fig. 7. Figure 7a depicts the time-of-flight data for two different pulse lengths, 10 and 100 μs, and for two different flow rates, 2.62 and 2.83 nL/s. The 100 μs pulse length increases the intensity of the larger *m/q* values in accordance with our modeling predictions and the Maxwell-Boltzmann distribution widens with higher *m/q* species detected. These pairs of spectra were obtained upon acquisition of the new pulsing setup, which allowed sequential measurement in which the only variable altered was the pulse length. The transmission function used to scale the data shown in Fig. 5a to the data illustrated in Fig. 5b was validated using this data and was in excellent agreement with that simulated. This transmission function is shown in the inset plot of Fig. 7b.

The time-of-flight spectra presented in Fig. 7c are the result of summation of the spectrum taken at each respective energy defect, as opposed to only presenting the results at one energy defect. The spectra have been scaled with the appropriate scaling function since much of the data was taken with 10 μs pulses. For comparison, the unscaled high mass range spectra is presented in Fig. 7b along with the transmission function. Similar to the IM-based liquids, the spectra contains small ion species, small *m/q* droplets, and large *m/q* droplets although the respective *m/q* values vary. At the low flow rates, the small *m/q* droplets are at their most intense, largest *m/q*, and widest distributions. These distributions narrow, become less intense, and begin to shift towards zero as the flow rate increases. The large *m/q* distribution extends out to approximately 200,000 amu/q and appears to increase in most probable *m/q* value as the flow rate increases. The singly-charged BMI-DCA ions can be identified out to $n = 13$ species (2804 amu/q) in the TOF data.

For the flow rate of 1.99 nL/s, individual spectrum acquired at selected defect energies are presented in Fig. 7d. Four different energy defects are pictured for the large mass droplets along with an associated fit for the large mass component of each trace in order to aid the reader. The noise increases at large *m/q* values as a result of the larger scaling factors employed in the transmission function as the *m/q* value increases. The peak of the fit is taken as the most probable *m/q* value for a given energy defect and this serves as the center value in the Maxwell-Boltzmann fits. As the energy defect increases, the most probable *m/q* value and the distributions' *m/q* range in general appear to shift to smaller and smaller *m/q* values. By an energy defect of 350 eV/q, the distribution encompasses a range of

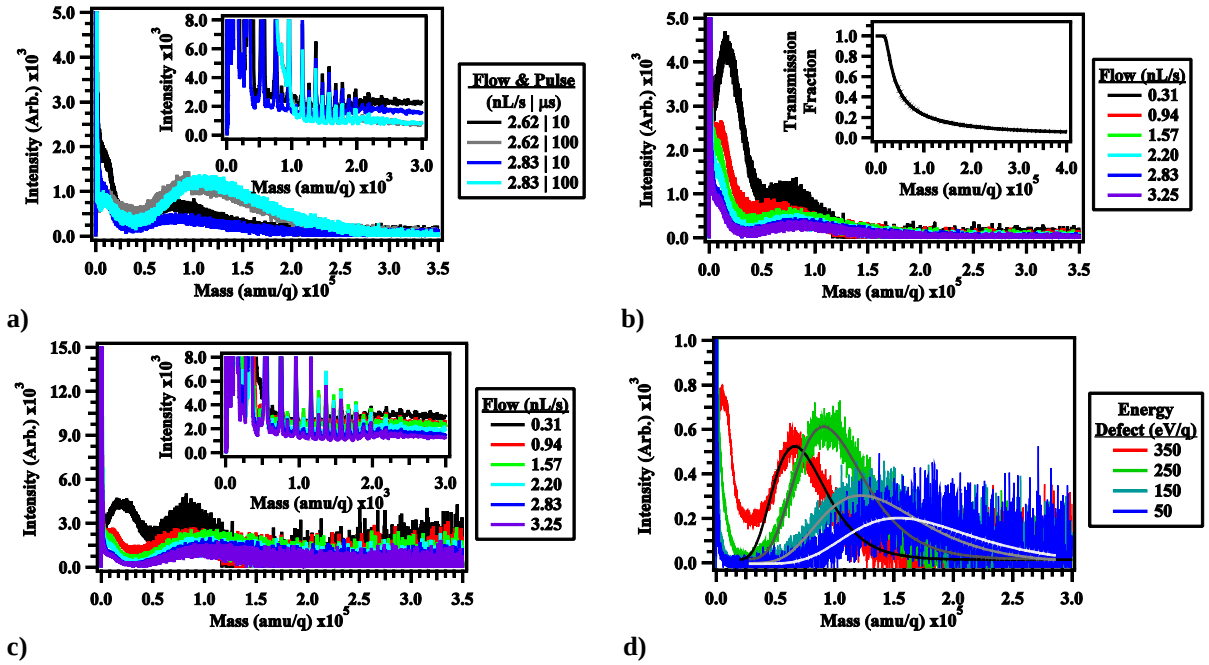

Figure 7. TOF cation mass spectra for the IL BMI-DCA. a) Mass spectra comparison of two different pulse lengths for two flow rates. The inset plot reveals the lower mass ions mass range under 3,000 amu/q. b) The inset plots shows the scaling transmission function used to modify mass spectra data and the main plot shows the unscaled summed spectra for various pulsing potentials using a 10 μs pulse length. c) Illustration of the scaled mass spectra. d) Individual spectrum acquired at selected defect energies at 1.99 nL/s.

approximately 43,000 to 102,000 amu/q (FWHM) whereas the 50 eV/q defect high mass droplet component included the region from 105,000 *m/q* to 226,000 amu/q (FWHM).

IV. Discussion

The TOF data serves as a large source of information regarding the charged species and their respective energy dependencies in ions present in the IL electrospray beam. The quadrupole data, despite the limited *m/q* range, aids the interpretation of the low *m/q* species observed in the TOF data. In Figs. 3 and 7, the same three distinct regions are present in the data for all three ILs for which TOF data was acquired. The singly-charged ion components, occurring at the lowest *m/q* values, of the electrospray beam have been easily identified in the spectra of either instrument's data set just by matching each peak's mass to the corresponding ion mass. The extended sequence of these ions appear to be present in all but the lowest volumetric flow rates sampled and generally at all energy defects. The second component consists of *m/q* values in the range of 6,000 amu/q to approximately 50,000 amu/q, which exhibit a significant flow rate and energy defect dependence in the presented results. The final component is composed of significantly large *m/q* values typically of order 100,000 amu/q and appears to have a flow rate and energy defect dependence. We first turn to discussing the ramifications of the energy defect results on the low and high mass droplet components. The energy defect dependence of two different ionic liquids at selected flow rates were presented in Figs. 5 and 7d. As is clear from the individual traces, the large mass droplet component consists of a wide *m/q* distribution at each trace, with the smallest *m/q* distribution occurring at the greatest energy defect and the largest *m/q* distribution occurring at the smallest energy defect in both cases. These distributions fit well to Maxwell-Boltzmann distributions, likely reflecting the statistical nature of the emitted products. Examples of these fits were included in Fig. 7d for the BMI-DCA IL as a visual aide. In Fig. 8, we plot the most probable *m/q* value of the distribution at a specific energy defect as a function of the energy defect for the two ILs along with a linear regression analysis. In all cases where this analysis has been performed, the most probable *m/q* value appears to exhibit a linear dependence with the energy defect. In all cases, the largest *m/q* droplets occur with the smallest energy defect while the smallest *m/q* droplets occur with the largest energy defect.

The TOF technique can identify the mass-to-charge (*m/q*) of both of the small and large droplet components but it cannot identify separately the mass or charge. A common assumption is to assume emitted droplets occur with charges of 44% of the Rayleigh limit. This assumption is applied to the integrated TOF mass spectra. The integrated EMI-IM data at a flow rate of 1.24 nL/s has a large droplet *m/q* value range of approximately 145,000 amu/q to 335,000 amu/q as measured by the FWHM of a Maxwell-Boltzmann distribution. This distribution would require droplets ranging in diameter from 25.8 nm to 45.1 nm with masses ranging from ~8.2 x 10^6 to 4.41 x 10^7 amu. This wide range of sizes, droplet masses, and the previously presented energy defect dependence suggests an alternative approach should be adopted. One such approach is to assume that the droplet mass is approximately fixed, and the distribution simply reflects the varying number of unique charges on this system, perhaps with the most probable *m/q* value of the entire droplet distribution reflecting the 44% Rayleigh limit.

This approach is detailed in Fig. 9 for EMI-IM at 1.24 nL/s. The integrated peak is generated by fitting a Maxwell-Boltzmann distribution to the sum of all of the individual energy defect TOF mass spectra (see Fig. 5b). The peak of the distribution is arbitrarily assigned a charge value equal to 44% of the Rayleigh limit. Equation (1) shows the calculation to obtain the droplet radius and mass using the 44% value. Here, ρ is the density of EMI-IM (1,519.3 kg/m^3), γ is the surface tension (0.0357 N/m), and ε_0 is the permittivity of free space. Setting the left hand side of Equation (1) to 220,540 amu/q and appropriately converting yields a droplet radius of 17.1 nm (diameter of 34.2 nm). An associated mass of 1.91 x 10^7 amu and Rayleigh charge limit of 197 charges for this droplet is determined by iteration of Equation (1). The Rayleigh charge limit of 197 charges is denoted by the second dashed line near 97,000 amu/q of Fig. 9. A fit to the large *m/q* component distributions for the energy defect of 100 eV/q and 300 eV/q is also shown in red and blue, respectively. As can be seen in Fig. 9, the Rayleigh limit roughly approximates the lowest *m/q* values observed in the large mass droplet component. As a result, it is expected a small distribution of droplet sizes, perhaps ± 1 nm, with a wide distribution of charges gives rise to the large *m/q* components observed for all

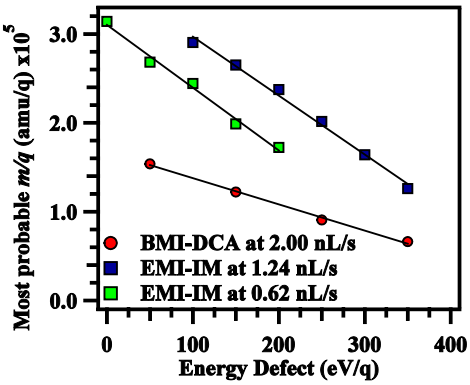

Figure 8. Most probable *m/q* value versus energy defect for selected ILs at selected flow rates and their respective linear fits.

ILs where TOF data was acquired at flow rates above 0.50 nL/s. Under the assumption that the large *m/q* components in the emitted beam are composed of a wide diversity of charge but a relatively narrow droplet size distribution, the energy defect data takes on additional meaning. The smaller energy defect droplets are consequently composed of the approximately fixed mass but with less of a net charge while the larger energy defect droplets contain larger net charges. We will revisit the implications of this finding in regards to emission from the jet towards the end of the discussion section.

$$\frac{m}{0.44q_{Ray}} = \frac{\rho(r_{Drop})^{\frac{3}{2}}}{6*0.44(\varepsilon_0\gamma)^{\frac{1}{2}}} \quad (1)$$

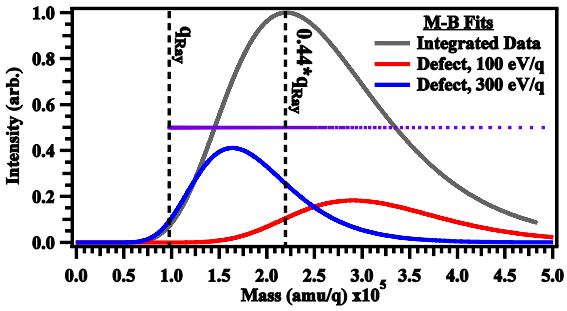

Figure 9. Maxwell-Boltzmann (M-B) fit to the large *m/q* component of EMI-IM at Q = 1.24 nL/s. The most probable *m/q* value has been arbitrarily assigned q = 0.44 * q_{Ray}. Fits to the large *m/q* component in the individual spectrum at energy defects of 100 eV/q and 300 eV/q are also shown. Purple dots indicate the *m/q* values expected for a fixed m and varied q.

The sequence of ion clusters in the low *m/q* region appears heavily dependent on the volumetric flow rate. At low flow rates below 0.20 nL/s, the results show only the smallest of the ion species present in the emitted beam. This is in agreement with the extensive body of literature on the ion species present in electrospray studies operated at the lowest volumetric flow rates. In those cases, the lowest volumetric flow rates are obtained by use of etched-metal needle emitters operating well below 0.20 nL/s. Figures 6 and 3b have mass spectrum for flow rates below 0.20 nL/s and in all cases, despite the differences in liquid makeup, all exhibit ion clusters most significant about the $n = 0$ and $n = 1$ ions. The quadrupole data presented in Fig. 4 for the anions of the IM-based ILs demonstrate the significant alteration that occurs between approximately 0.30 nL/s and 0.50 nL/s as the smallest ion populations significantly decrease to be replaced by intensity in slightly larger clusters, which also decrease as the volumetric flow rate continues to increase.

At flow rates above 0.20 nL/s, the evidence in the TOF results indicates that multiply-charged ions are present even at *m/q* values below 3,700 amu/q in the emitted beam. For example, in Fig. 3b, there is a distinct peak occurring at 3,043 amu/q that corresponds to the mass of a doubly-charged EMI-IM ion. Specifically, it represents a doubly charged ion with 2 EMI^+ ions and 15 neutral pairs of EMI-IM. The remaining unknown peaks extending to higher masses represent the odd numbered neutral pairs of EMI-IM (i.e. 17, 19, 21, etc.) joined with 2 EMI^+ ions. The even numbered neutral pairs overlap with the singly-charged ion peaks. As a result, the singly-charged ion peak intensity represents the combination of the detected singly-charged and doubly-charged ion intensities in this region of the mass spectra. For BMI-IM in Fig. 3a, the IL shares the same minimum doubly-charged species as EMI-IM. This doubly-charged ion of 15 neutrals with 2 BMI^+ ions has a mass of 3,281 amu/q. Again, the extension of peaks to higher masses represent the odd numbered neutral pairs of BMI-IM. The BMI-DCA shows the same singly/doubly-charged sequence, but these peaks occur in the spectra at much lower masses (see Fig. 7a). For BMI-DCA, the first clearly defined unidentified peak occurs at 856 amu/q. This *m/q* value corresponds to the mass of 7 neutral pairs of BMI-DCA and 2 BMI+ ions. Again, the iteration of peaks is the odd numbered neutral pairs of the doubly-charged ions.

The collected data provided by the quadrupole instrument shares the same pattern of doubly-charged ions within the limited mass scanning range. For BMI-IM and EMI-IM, the cation data (not shown in this paper) show the doubly-charged ions begin at the *m/q* values representing 15 neutral pairs and two cations of the ILs. In the anion data of Fig. 4, the doubly-charged ions sequence starts to grow in the spectra at the 2,584 amu/q peak (11 neutral pairs and 2 IM^- ions) for BMI-IM and at the 2,430 amu peak (11 neutral pairs and 2 IM^- ions) for EMI-IM. In the anion spectra of EMI-IM, the 2,430 amu peak is faint as presented, but the doubly-charged ions are clearly indicated by the 2,821 amu/q mass peak (13 neutral pairs and 2 IM^- ions).The BMI-BF_4 cation and anion quadrupole data faintly indicate the presence of doubly-charged ions also. Doubly-charged cations start at 1,834 amu/q (15 neutral pairs with 2 BMI^+ ions) and the doubly-charged anions start at 15,56 amu/q (13 neutral pairs with 2 BMF_4^- ions). Once a full set of BMI-BF_4 TOF scans are complete, it is expected the same pattern will appear in the spectra as clearly as with BMI-IM, EMI-IM, and BMI-DCA data.

While singly and doubly-charged species are easily assignable between the two measurement techniques, it is difficult to directly assign triply-charged ions in the TOF spectra of the ILs. If triply-charged ions are resolvable, a mass peak on each side of the doubly-charged ions is expected in the scans. Based on the data, a few of the doubly-charged ion peaks seem to broaden or have shoulders at higher flow rates; however, there are no distinct peaks that

do not fall on a doubly-charged mass. In the EMI-IM data (Fig. 3b), the ion at 4,607 amu/q appears to be the starting point for broader peaks. It is possible this broadening could be a starting point for triply-charged ions or simply be the result of the decrease in resolution that occurs as more and more atoms constitute a larger ion cluster. Unfortunately, the orthogonal TOF technique employed in this work does allow a transverse velocity distribution that results from extraction of the ions from different locations in the extraction region. This results in the somewhat broader linewidths observed even for the smallest ion clusters. Nonetheless, presence of doubly-charged ions typically correlates with a "plateau" feature appearing at *m/q* values exceeding 4,000 amu/q where it is difficult to definitively assign any ion, although real ion signal is present. The failure to resolve ion clusters in these plateaus leaves us only with the speculation that there are many different ion clusters with multiple net charges composing this region, likely including triply-charged and more highly-charged species.

The low mass droplets constitute the region near this plateau region and often include *m/q* values ranging from approximately 5,000 amu/q up until ~60,000 amu/q in IM-based ILs and ~30,000 amu/q in the BMI-DCA. The volumetric flow rate trend is best conveyed in Figs. 7c and 3 where, above 0.25 nL/s, the low mass droplet component often appears at its most intense and most broad distribution at the lowest flow rates. As the flow rate is increased, the intensity decreases and the distribution becomes less expansive for all ILs for which TOF data are available. This component also exhibits an energy defect dependence on the species present, although it appears opposite to that found for the large mass droplets. In Fig. 7d, the low mass droplet component extends to greatest *m/q* values at the largest energy defects and have almost no intensity at the smallest energy defects. As will be noted below, these low mass droplet species appear at all angles in the emission process in contrast to the large mass droplets. Since we cannot resolve species in this distribution, we tentatively note that the largest *m/q* values appear at the largest energy defect. We currently speculate that the species of this distribution likely experience emission from less intense electric fields present on the surface of the jet structure. Within this tentative explanation, the narrowing of the distribution reflects that, at smaller energy defects, the electric field is more significant and leads to dissociation from the cone-jet structure or possibly from the larger *m/q* components. These species are apparent on the lower *m/q* side of this low mass distribution.

In the preliminary work on BMI-DCA, the large mass droplet distribution only occurred along the centerline of the electrospray beam while the low mass droplet and ion species were observed even when the source was rotated to higher angle (i.e. source rotated to 30° and 45°). Given the angular dependence of the high mass distribution and the linkage of the charge on these species to the Rayleigh limit, we believe the high mass component results from droplet ejection due to the jet breakup by a Rayleigh instability.[24] The beam axis dependence indicate that the droplet component of the electrospray beam is due to a varicose type instability that produces uniform sized droplets in line with the jet structure along the beam centerline. In a varicose instability, the jet becomes pinched into small segments along the jet length. Once the amplitude of the instability exceeds the jet radius, the pinched segments break off with each segment length corresponding to the wavelength of the instability. An *m/q* distribution results from the droplet breakup due to a uniform sized or consistent mass, on the order of million's of amu, being ejected, but the charge condition in each segment is variable. The combination of the angular dependence and the energy defect analysis is illuminating since the existence of a potential dependence suggests that large droplets do not only emit from a static jet tip at a given length. Instead, these ejected droplets assume the potential corresponding to their respective location in the jet, and the energy distribution results from multiple droplets emitting simultaneously, from various locations, in the stressed jet.

V. Conclusion

This study explored the mass spectrometry of a variety of ILs electrosprayed with a capillary emitter with a particular emphasis on large *m/q* species and the energy dependence of emitted ions over a volumetric flow rate range of 10's of pL/s to a couple nL/s. The investigations examined ILs with different cation and anion components to provide a more generalized comparison of the resulting mass spectra and to evaluate for common trends. Above flow rates of 0.25 nL/s, all of the sampled ILs exhibited similar compositional trends although the relevant *m/q* values were different. The TOF spectra of these ILs at the higher flow rates consisted of ions in three distinct regions: small ions composed of net singly- and doubly-charged ion clusters, low mass droplets characterized by a Maxwell-Boltzmann distribution typically in the region of 10,000 to 60,000 amu/q with an unknown number of charges, and a large mass droplet characterized by a wide distribution of *m/q* values. Analysis of the large mass droplet components appears in agreement with the Rayleigh limit approach often used for macroscale droplets, notably, assuming the most probable value of the large mass droplet is occurring with approximately 44% of the Rayleigh limit charge. The energy-selected TOF mass spectra suggest that the large mass droplet distribution is actually composed of various *m/q* distributions unique to the energy defect. Notably, the largest *m/q* values in the large droplet distribution occur at the smallest

energy defects and the most probable *m/q* value varies linearly with the energy defect. We have preliminarily assigned this behavior to emission of large droplets down the center beam axis in a concerted manner; those droplets with greatest defect, and greatest net charge, emit from the jet most closely to the jet tip while those with smaller energy defects, and net charge, emitting in the jet breakup closer to the Taylor cone.

Acknowledgments

This work was supported by AFOSR task 16RVCOR275 (Program Manager: Michael Berman)

References

[1] Dambach, E., Heister, S., Ismail, I., Schneider, S. and Hawkins, T. W., "An Investigation into the Hypergolicity of Dycanamide-based Ionic Liquid Fuels with Common Oxidizers," Air Force Research Laboratory, Edwards Air Force Base, CA, *55th JANNAF Propulsion Meeting/4th Liquid Propulsion Subcommittee/3rd Spacecraft Propulsion Subcommittee/6th Modeling and Simulation Subcommittee Meeting*, Orlando, FL, TP-2008-371, 2008.

[2] Hruby, V., Spence, D., Demmons, N., Roy, T., Ehrbar, E., Zwahlen, J., Martin, R., Ziemer, J., Connolly, W., Rhodes, S. and Tolman, W., "ST7-DRS Colloid Thruster System Development and Performance Summary," *44th AIAA/ASME/SAE/ASEE Joint Propulsion Conference & Exhibit*, Hartford, CT, AIAA Paper 2008-4824, 2008.

[3] Gamero-Castaño, M. and Hruby, V., "Characterization of a Colloid Thruster Performing in the Micro-Newton Thrust Range," *27th International Electric Propulsion Conference*, Pasadena, CA, 2001.

[4] Ziemer, J. K., Gamero-Castaño, M., Hruby, V., Spence, D., Demmons, N., McCormick, R., Roy, T., Gasdaska, C., Young, J. and Connolly, W., "Colloid Micro-Newton Thruster Development for the ST7-DRS and LISA Missions," *41st AIAA/ASME/SAE/ASEE Joint Propulsion Conference & Exhibit*, Tucson, AZ, AIAA Paper 2005-4265, 2005.

[5] "MIT SPL Delivers the Scalable ion Electrospray Propulsion System (S-iEPS) for CubeSats to NASA," July 2, 2015, <http://web.mit.edu/aeroastro/labs/spl/iEPS_NASA.html> (June 10, 2016).

[6] Lozano, P. C., "Energy Properties of an EMI-Im Ionic Liquid Ion Source," *Journal of Physics D: Applied Physics*, Vol. 39, No. 1, 2006, pp. 126-134.

[7] Chiu, Y., Gaeta, G., Levandier, D. J., Dressler, R. A. and Boatz, J. A., "Vacuum Electrospray Ionization Study of the Ionic Liquid, [Emim][Im]," *International Journal of Mass Spectrometry*, Vol. 265, No. 2-3, 2007, pp. 146-158.

[8] Ticknor, B. W., Anderson, J. K., Fritz, B. A. and Chiu, Y.-H., "Effect of Aspect Ratio on the Wettability and Electrospray Properties of Porous Tungsten Emitters with the Ionic Liquid [Emim][Im]," *46th AIAA/ASME/SAE/ASEE Joint Propulsion Conference & Exhibit*, Nashville, TN, AIAA Paper 2010-6618, 2010.

[9] Ticknor, B. W., Miller, S. W. and Chiu, Y. H., "Mass Spectrometric Analysis of the Electrospray Plume from an Externally Wetted Tungsten Ribbon Emitter," *45th AIAA/ASME/SAE/ASEE Joint Propulsion Confernce & Exhibit*, Denver,CO, AIAA Paper 2009-5088, 2009.

[10] Miller, S. W., Prince, B. D. and Rovey, J. L., "Capillary Extraction of the Ionic Liquid [Bmim][DCA] for Variable Flow Rate Operations," *48th AIAA/ASME/SAE/ASEE Joint Propulsion Conference & Exhibit*, Atlantia, GA, AIAA Paper 2012-3738, 2012.

[11] Miller, S. W., Prince, B. D., Bemish, R. J. and Rovey, J. L., "Electrospray of 1-Butyl-3-Methylimidazolium Dicyanamide Under Variable Flow Rate Operations," *Journal of Propulsion and Power*, Vol. 30, No. 6, 2014, pp. 1701-1710.

[12] Terhune, K. J., King, L. B., Prince, B. D. and Hawkett, B. S., "Species Measurements in the Beam of an Ionic Liquid Ferrofluid Capillary Electrospray Source," *52nd AIAA/SAE/ASEE Joint Propulsion Conference*, Salt Lake City, UT, 2016.

[13] Chiu, Y., Austin, B., Dressler Rainer, A., Levandier, D., Murray, P. T., Lozano, P. and Martinez-Sanchez, M., "Mass Spectrometric Analysis of Colloid Thruster Ion Emission from Selected Propellants," *Journal of Propulsion and Power*, Vol. 21, No. 3, 2005, pp. 416-423.

[14] Berg, S. P. and Rovey, J. L., "Assessment of Multi-Mode Spacecraft Micropropulsion Systems," *50th AIAA/ASME/SAE/ASEE Joint Propulsion Conference*, Cleveland, OH, AIAA Paper 2014-3758, 2014.

[15] Chiu, Y., Levandier, D., Austin, B., Dressler Rainer, A., Murray, P. T., Lozano, P. and Martinez-Sanchez, M., "Mass Spectrometric Analysis of Ion-Emission from Selected Colloid Thruster Fuels," *39th AIAA/ASME/SAE/ASEE Joint Propulsion Conference and Exhibit*, Huntsville, AL, AIAA Paper 2003-4848, 2003.

[16] Chiu, Y., Gaeta, G., Heine, T. R., Dressler, R. A. and Lavandier, D. J., "Analysis of the Electrospray Plume from the EMI-Im Propellant Externally Wetted on a Tungsten Needle," *42nd AIAA/ASME/SAE/ASEE Joint Propulsion Conference & Exhibit*, Sacramento, CA, AIAA Paper 2006-5010, 2006.

[17] Tokuda, H., Tsuzuki, S., Susan, M. A. B. H., Hayamizu, K. and Watanabe, M., "How Ionic Are Room-Temperature Ionic Liquids? An Indicator of the Physicochemical Properties," *The Journal of Physical Chemistry B*, Vol. 110, No. 39, 2006, pp. 19593-19600.

[18] Jacquemin, J., Husson, P., Padua, A. A. H. and Majer, V., "Density and Viscosity of Several Pure and Water-Saturated Ionic Liquids," *Green Chemistry*, Vol. 8, No. 2, 2006, pp. 172-180.

[19] Huddleston, J. G., Visser, A. E., Reichert, W. M., Willauer, H. D., Broker, G. A. and Rogers, R. D., "Characterization and Comparison of Hydrophilic and Hydrophobic Room Temperature Ionic Liquids Incorporating the Imidazolium Cation," *Green Chemistry*, Vol. 3, No. 4, 2001, pp. 156-164.

[20] Liu, W., Zhao, T., Zhang, Y., Wang, H. and Yu, M., "The Physical Properties of Aqueous Solutions of the Ionic Liquid [BMIM][BF4]," *Journal of Solution Chemistry*, Vol. 35, No. 10, 2006, pp. 1337-1346.
[21] Sanmamed, Y. A., González-Salgado, D., Troncoso, J., Cerdeiriña, C. A. and Romaní, L., "Viscosity-Induced Errors in the Density Determination of Room Temperature Ionic Liquids using Vibrating Tube Densitometry," *Fluid Phase Equilibria*, Vol. 252, No. 1–2, 2007, pp. 96-102.
[22] Nishida, T., Tashiro, Y. and Yamamoto, M., "Physical and Electrochemical Properties of 1-Alkyl-3-Methylimidazolium Tetrafluoroborate for Electrolyte," *Journal of Fluorine Chemistry*, Vol. 120, No. 2, 2003, pp. 135-141.
[23] Donius, B. R., "Investigation of Dual-Mode Spacecraft Propulsion by Means of Ionic Liquids," Masters Thesis, Mechanical and Aerospace Engineering Dept., Missouri University of Science and Technology, Rolla, MO, 2010.
[24] Rayleigh, L., "On the Instability of Jets," *Proceeding of the London Mathematical Society*, Vol. 10, No. 1878, pp. 4-13.